Topological Protection Brought to Light by the Time-Reversal Symmetry Breaking

S. U. Piatrusha,[1] E. S. Tikhonov,[1,2,*] Z. D. Kvon,[3,4] N. N. Mikhailov,[3,4] S. A. Dvoretsky,[3] and V. S. Khrapai[1,5]

[1]*Institute of Solid State Physics, Russian Academy of Sciences, 142432 Chernogolovka, Russian Federation*
[2]*National Research University Higher School of Economics, Moscow 101000, Russian Federation*
[3]*Institute of Semiconductor Physics, Novosibirsk 630090, Russian Federation*
[4]*Novosibirsk State University, Novosibirsk 630090, Russian Federation*
[5]*Moscow Institute of Physics and Technology, Dolgoprudny, 141700 Russian Federation*

Recent topological band theory distinguishes electronic band insulators with respect to various symmetries and topological invariants, most commonly, the time reversal symmetry and the Z_2 invariant. The interface of two topologically distinct insulators hosts a unique class of electronic states—the helical states, which shortcut the gapped bulk and exhibit spin-momentum locking. The magic and so far elusive property of the helical electrons, known as topological protection, prevents them from coherent backscattering as long as the underlying symmetry is preserved. Here we present an experiment that brings to light the strength of topological protection in one-dimensional helical edge states of a Z_2 quantum spin-Hall insulator in HgTe. At low temperatures, we observe the dramatic impact of a tiny magnetic field, which results in an exponential increase of the resistance accompanied by giant mesoscopic fluctuations and a gap opening. This textbook Anderson localization scenario emerges only upon the time-reversal symmetry breaking, bringing the first direct evidence of the topological protection strength in helical edge states.

Bloch's quantum mechanical band theory states that electronic waves propagate freely in a periodic lattice of a crystalline solid [1]. A defect of any kind breaks the translational symmetry of the lattice and mediates scattering, similar to the diffraction of plane waves in a defected continuous medium. With an increasing number of defects, the free propagation of a wave turns into a diffusion. Given the phase coherence is preserved, the constructive interference between the time-reversed random diffusion paths gives rise to a coherent backscattering of a wave. This genuine quantum effect is observed as a narrow resonance in the intensity of light backscattered off a milky solution [2–4] and as a weak localization correction to the conductance of a diffusive metal [5]. Eventually, in a sufficiently disordered system, the coherent propagation gets suppressed, be it light [6,7], electron [8], or even sound [9] or matter waves [10,11]—the phenomenon known as Anderson localization [12,13]. For the helical states, however, the situation inverts thanks to a destructive interference of the time-reversed paths. Thereby the free propagation is maintained in the presence of a symmetry-conserving disorder, which is known as topological protection [14,15].

Helical edge states represent a unique example of a 1D electronic system, which can only be realized at the interface of a two-dimensional (2D) Z_2 topological and trivial insulators [15], in this work it is the quantum spin-Hall (QSHI) insulator in HgTe/CdHgTe quantum wells (QWs) with the inverted band structure and vacuum [16]. Spin-momentum locking is manifested in two counter-propagating opposite-spin species at each edge of a planar device, which provide the only transport channel when the Fermi level is tuned within the 2D bulk energy gap [17]. Numerous direct consequences of this physical picture are corroborated experimentally, including the observation of quantized conductance $G \approx G_0 \equiv e^2/h$ of the shortest edge channels [17–19], nonlocal transport in zero magnetic field [19–24], positive magnetoresistance [17,25], the spin-charge sensitivity [26] and the unconventional behavior in lateral *p-n* junctions [24,27].

In spite of the impressive progress, the mean-free path of the helical electrons is typically disappointingly small [17,19–23,28–32], even compared to the conventional high-purity 1D conductors [33]. The puzzles of the trivial Ohmic behavior and weak or even absent temperature dependence [17,19,28–32,34,35] along with the nearly universal partition noise [35–37] further indicate that the edge transport beyond the mean-free path in zero magnetic field is classical, rather than quantum coherent, by nature. As a matter of fact, the advantages offered by the concept of topological protection, which are of paramount importance for numerous applications [38,39], were so far hidden by an extremely efficient phase-breaking mechanism of a debated origin [40–46]. Here, we approach this problem from a different perspective, using coherent backscattering as a marker for a breakdown of the topological protection.
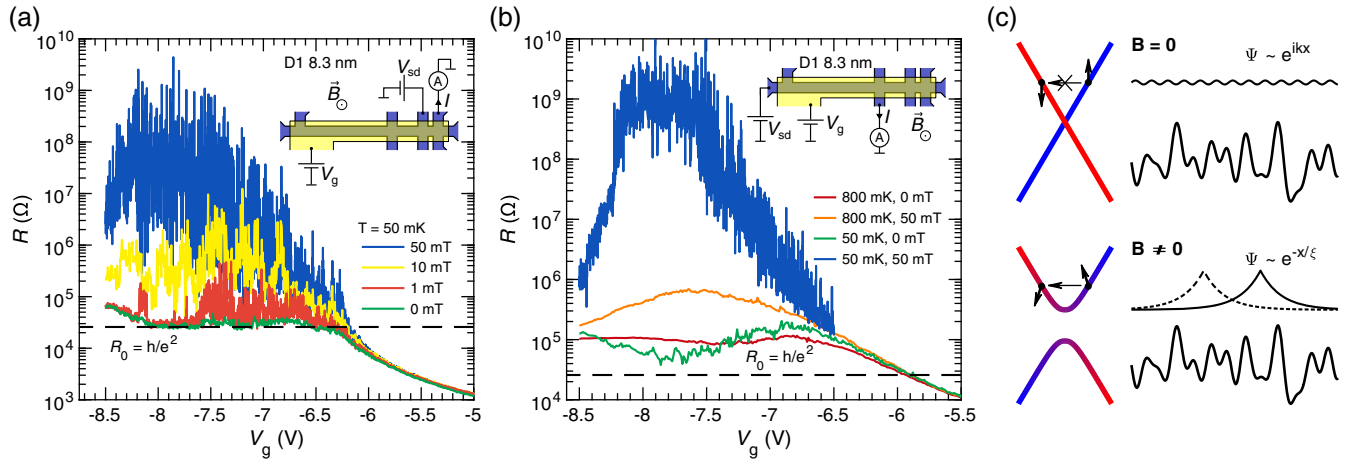
FIG. 1.   Two-terminal characteristics of the QSHI device. (a) Two-terminal linear-response resistance of the 6 μm-long edge in $D1$ (8.3 nm QW) as a function of the gate voltage, measured at $T = 50$ mK in different magnetic fields $B_\perp$. (b) Two-terminal linear-response resistance of the 38 μm-long edge in $D1$ as a function of the gate voltage, measured at $T = 50$ and $T = 800$ mK, with and without magnetic field $B_\perp = 50$ mT. The insets on (a) and (b) show device structures along with measurement schematics. (c) Effect of the magnetic field on electronic states in QSHI. If $B = 0$, a gapless energy spectrum with spin-momentum locking (top left) is expected, while the propagating electrons are not influenced by potential disorder (top right). The electron wave function Ψ corresponds to free propagation along the edge [48], $\Psi \sim e^{ikx}$. At nonzero B the gap opens while the counterpropagating branches are no longer comprised of states with opposite spins (bottom left). Eventually, the disorder leads to backscattering and localizes the electrons (bottom right) with their wave function envelope decaying exponentially over the localization length ξ, $\Psi \sim e^{-x/\xi}$.

We observe that the time-reversal symmetry (TRS) breaking by magnetic field restores the coherent backscattering, thereby drastically decreasing the mean-free path in a finite magnetic field, and drives the Anderson localization of the helical edge channels. This behavior unveils the actual strength of the topological protection in the TRS case.

We investigate two QSHI devices of different crystallographic orientation and QW thickness d. In device $D1$, the QW with $d = 8.3$ nm resides in a (013) plane, while the device $D2$ is based on the (112) QW with $d = 14$ nm. We note that the QWs of both devices are similar in design to the QWs studied in Refs. [19,25]. Both devices are shaped as multiterminal Hall bars with Ti/Au metallic top gates, see insets of Figs. 1(a) and 1(b) for the schematic representation of the device and measurement configuration. The microscope image of one of the devices may be found in the Supplemental Material [47], Fig. 1. For additional device fabrication and measurement technique details see corresponding sections of the Supplemental Material [47].

Using the gate voltage V_g, the Fermi level can be tuned within the bulk energy gap, as large as 30 meV in $D1$ and 3 meV in $D2$ [16,19]. In this way the QSHI regime is realized, with the predominant edge conduction confirmed by transport measurements in similar devices [19,24,28,35] and, independently, here via nonlocal resistance measurements (see Supplemental Material [47], Fig. 3). Various distances between the neighboring Ohmic contacts allow us to choose the different lengths of the edge channels, spanning the range between 2 and 38 μm in each device, with edge resistance increasing with increasing edge

length. The device $D1$ demonstrates resistance $R \approx R_0 \equiv h/e^2$ for the shortest edges, while in $D2$ the resistance is about twice as large for the same edge length (see Supplemental Material [47], Figs. 9, 11). In the following we discuss the results obtained for device $D1$. Similar data obtained for device $D2$ are demonstrated in the Supplemental Material.

Figures 1(a) and 1(b) show the two-terminal resistance of the 6 and 38 μm-long edges in $D1$, with subtracted contribution of contact terminals, as a function of V_g in a magnetic field perpendicular to the QW plane $B_\perp$. The measurement configurations are shown in the corresponding insets. For the two-terminal resistance of an N-terminal device in the phase-coherent case, Landauer-Buttiker analysis [49] would yield $R_0(1 - 1/N)$, which in our case is $\approx 0.9R_0$. This reasoning, however, is not applicable in our experiment since the edges longer than 6 μm are in the phase-incoherent regime.

For $B_\perp = 0$ at $T = 50$ mK, within the range of gate voltages -8 V $< V_g < -6.5$ V the 6 μm-long edge demonstrates the conductance plateau with the value close to G_0 and the device demonstrates the nonlocal resistance (see Supplemental Material [47], Fig. 3), which corresponds to the onset of the QSHI regime. At the same time, no sizable T dependence is observed, which is usual for the QSHI edges [29,34,35]. By contrast, in a small magnetic field of $B_\perp = 50$ mT the resistance increases dramatically, sometimes reaching $R \sim 1$ GΩ in $B_\perp = 50$ mT at $T = 50$ mK. Qualitatively similar but even stronger effect of the magnetic field is observed in the longer 38 μm edge, as shown in Fig. 1(b). As the temperature is raised to $T = 800$ mK,

the resistance drops down again by more than a factor of 10^3. The straightforward cross-check demonstrates that in all our measurements the current flows along the edges of the device, while the bulk conduction contribution remains negligible even for $R \sim 1$ GΩ (see Supplemental Material [47], Fig. 4). All the edges of both our devices $D1$ and $D2$ exhibit the reported resistance increase in a small magnetic field, which is also the case for the four-terminal configuration measurements (see Supplemental Material [47], Figs. 9–12 for additional data).

Figures 1(a) and 1(b) highlight our main result that a tiny magnetic field gives rise to the dramatic increase of the resistance of the helical edge states accompanied by strong T dependence and highly reproducible, giant mesoscopic fluctuations (see Supplemental Material [47], Fig. 5). Altogether, this behavior is a hallmark of the Anderson localization of the electronic states and manifests a transition from the topologically protected phase to the trivial insulator in a magnetic field as anticipated in various scenarios [48,50,51]. The underlying microscopic explanation is depicted in Fig. 1(c). In $B = 0$, the dispersion relation of the helical electrons consists of two opposite spin counterpropagating branches, the coherent backscattering between which is forbidden by the topological protection [15]. In a finite B field, the branches hybridize, opening an energy gap in the vicinity of the Dirac point, and the spins of the counterpropagating electrons acquire a common tilt along the magnetic field. Thus, the coherent backscattering mediated by potential disorder is restored in the magnetic field, resulting in Anderson localization of the electronic states on the length scale of the mean-free path, in contrast to the $B = 0$ case.

It is important to emphasize that both short edges with $G \approx G_0$ and the longer ones with $G < G_0$ behave similarly in finite B. Breaking the TRS with magnetic field allows coherent backscattering in both cases, leading to the helical edge states localization. In this scenario, the observation of $G < G_0$ for long edges in the TRS case is due to phase breaking of the origin yet to be explained [40–46,52,53], while the absence of localization in zero magnetic field for resistive edges manifests the topological protection.

We now discuss in detail the T dependence of the QSH edge conductance $G = 1/R$ under broken TRS. As seen from Fig. 2, in the absence of magnetic field the T dependence within the charge neutrality point (CNP) region is of metallic type with approximately 20% change of the 6 μm-long edge resistance as T is reduced from 800 to 50 mK. For the 38 μm-long edge, within the range of gate voltages -8.3 V $< V_g < -7.4$ V we observe even stronger metallic behavior with a twofold decrease of resistance in the same T interval. We are not aware of similar observations in HgTe QWs, where the reported T dependencies are usually either completely absent or weakly insulating. We note, however, that most of the studies discuss $R(V_g)$ dependencies at temperatures above 1 K. Additionally, we
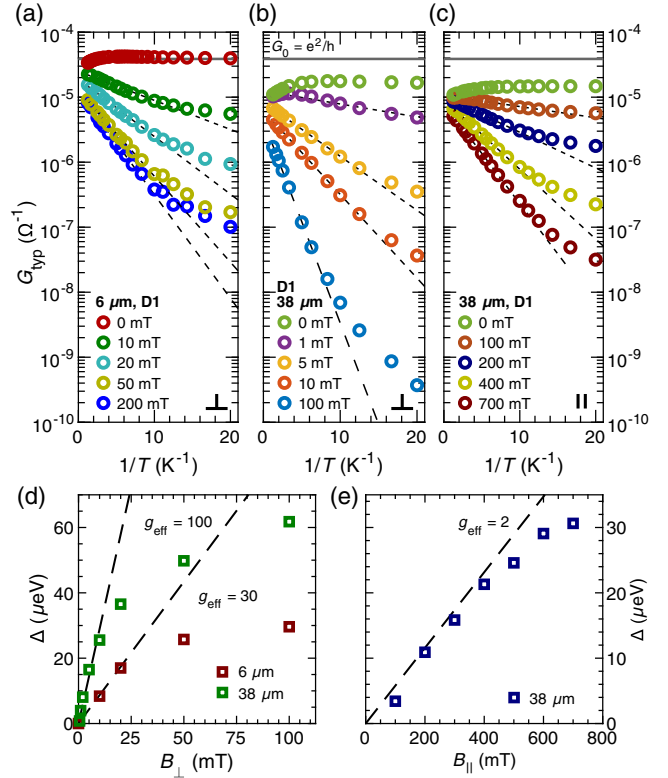

FIG. 2. Temperature and magnetic field dependence of the edge conductance in the localized regime. Log-averaged conductance G_{typ} (see text) as a function of inverse temperature of the (a) 6 μm-long edge in $D1$ and of the (b),(c) 38 μm-long edge in $B_\perp$ and $B_\parallel$, oriented at 45° to the edge, respectively. Application of magnetic field leads to the activationlike $G_{\mathrm{typ}}(T)$, in contrast to the weak metallic $G_{\mathrm{typ}}(T)$ in $B = 0$. The strong anisotropy with respect to the B orientation is evident. Solid lines demonstrate the conductance quantum value G_0. Panels (a)–(c) share the same y axis. Slight difference between zero-field data in panels (b),(c) is due to thermal recycling. The example of raw data is presented in the Supplemental Material [47], Fig. 7. (d) Activation energy Δ (see text) as a function of $B_\perp$, extracted from measurements in (a),(b). The dashed lines demonstrate the magnitude of the effect and are $2\Delta = g_{\mathrm{eff}}\mu_B B_\perp$ with the specified values of g_{eff}. (e) The same as (d), but for the 38 μm-long edge in $B_\parallel$, extracted from measurements in (c).

note that in $D2$, as well as for the 38 μm-long edge in $D1$ within the range of gate voltages -7.4 V $< V_g < -6.5$ V, the $R(T)$ dependence in $B = 0$ is of weakly insulating type at any V_g (see Supplemental Material [47], Fig. 6).

The $G(T)$ dependence in a magnetic field is much more impressive. In the presence of strong fluctuations, we analyze the log-averaged (typical) [54] conductance $G_{\mathrm{typ}} \equiv G_0 \exp \langle \ln G/G_0 \rangle$, with the averaging performed over the small gate-voltage region -7.65 V $< V_g <$ -7.55 V within the resistance maximum in Fig. 1(b). This relatively narrow range of V_g is chosen in order to resolve the fine structure of mesoscopic fluctuations in the vicinity of V_g value where the $G(T)$-dependence is

prominent enough, as reflected by the gate voltage dependence of the activation energy (see Supplemental Material [47], Fig. 8). The resulting data is shown in Figs. 2(a)–2(c). Strikingly, already for $B_\perp \sim 1$ mT the trend of $G_{\mathrm{typ}}(T)$ changes from metallic to activated insulating dependence $G_{\mathrm{typ}} \propto \exp(-\Delta/k_B T)$ (the remnant B field did not exceed 2 mT and was compensated in the experiment with 0.1 mT precision). The activation energy reaches about $\Delta \approx 10\ \mu$eV in 10 mT for the $6\ \mu$m-long edge, shows a sublinear increase with $B_\perp$, and increases with the length of the edge, Fig. 2(d). Thus, it is difficult to make an obvious relation of the activated behavior with the single-particle spectrum of the helical edge states, e.g., with a Zeeman gap opening at the Dirac point. Similar observations hold for the in-plane orientation of the magnetic field, see Figs. 2(c), 2(e) for the case of $B_\parallel$ directed at about 45° with respect to the edge under study. Here, the magnetic fields $B_\parallel$ roughly an order of magnitude stronger are required to observe the activated behavior comparable to the $B_\perp$ case. This might be a consequence of the Lande g-factor anisotropy predicted for HgTe QWs in some works [48].

We now quantitatively analyze the observed giant conductance fluctuations, which are the distinctive feature of the Anderson localized phase. Here, in contrast to the metallic phase, the conductance is exponentially sensitive to the minor variations of disorder, or equivalently, to the Fermi energy. As a result, the fluctuations of the conductance are as large as the average value and obey the log-normal distribution; i.e., it is the quantity $\ln G/G_0$ which is Gaussian distributed [54]. In Fig. 3 we study the conductance fluctuations as a function of magnetic field at various T. The square root of the normalized variance of the logarithm of the conductance, given by $\sqrt{-\mathrm{Var}(\ln G/G_0)\langle \ln G/G_0 \rangle^{-1}}$, is plotted in panels (a), (b) for short and resistive edges in $B_\perp$ and in panel (c) for resistive edge in $B_\parallel$. At the lowest available $T = 50$ mK it increases by more than 1 order of magnitude, compared to the $B = 0$ case, for $B_\perp \approx 20$ mT and $B_\parallel \approx 500$ mT. Still, the observed values are below the theoretical value of $\sqrt{2}$, which would correspond to a quantum-coherent Anderson localized phase [54]. We attribute the difference to the impact of averaging in the presence of dephasing [40–46], which also qualitatively explains the strong T dependence of the fluctuations in Fig. 3. The stronger fluctuations in the shorter edge further support this suggestion.

To further characterize the transport properties of the localized states, we study the nonlinear transport regime originating from the delocalization of the edge states by the electric field [55,56] for the $38\ \mu$m-long edge in $D1$ at $T = 50$ mK. The dependence of I on V_{sd} and V_g is plotted in panels (a) and (b) of Fig. 4 for $B_\perp = 100$ and $B_\parallel = 100$ mT, respectively. Within the CNP region one can see the dramatic changes in I at increasing $|V_{\mathrm{sd}}|$
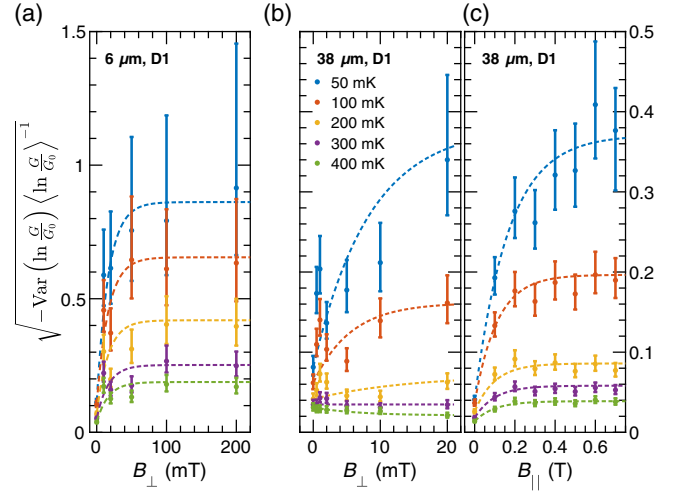

FIG. 3. Conductance fluctuations in the localized regime and its temperature dependence. Square root of the normalized variance of the logarithm of the edge conductance (see text) of the (a) $6\ \mu$m-long edge in $D1$ as a function of $B_\perp$ and of the (b), (c) $38\ \mu$m-long edge as a function of $B_\perp$ and $B_\parallel$. The confidence intervals are due to statistical analysis assuming the log-normal distribution of the conductance. The peak at lowest magnetic fields in panel (b) is most likely due to the sudden change of the state of the scatterers for a given edge. Dashed lines are guides for the eye. Panels (b) and (c) share the same y axis.

(note the log scale). Below the certain threshold value of V_{sd}, which depends on V_g with pronounced reproducible fluctuations above that, we observe only the negligible current $|I| < 1$ pA through the edge. For the magnetic field of 100 mT, the typical bias range of suppressed conduction changes from about 0.5 mV in $B_\perp$ to about
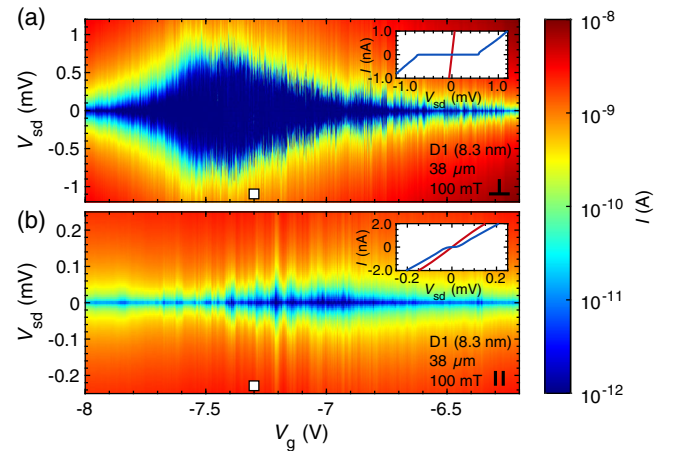

FIG. 4. Gap opening in the edge by the external magnetic field. (a) Current, flowing through the $38\ \mu$m-long edge of $D1$ as a function of gate and bias voltages in $B_\perp = 100$ mT. Measured current is plotted as a logarithm of its absolute value (see text). The inset demonstrates I-V_{sd} curves, measured at $V_g = -7.3$ V (white square) in $B_\perp = 0$ (red line) and 100 mT (blue line). (b) The same as (a) for $B_\parallel = 100$ mT, oriented at 45° to the edge.

50μV in $B_{\parallel}$. For this threshold, the corresponding energy scale is considerably higher than the activation energy extracted from the T dependencies similar to that of Fig. 2, indicating that the applied bias is shared among a few strongly localized electronic states along the edge. For the case of metal-insulator transition in Si inversion layers similar reasoning was suggested in Ref. [55]. Above the threshold, the conduction reasonably comparable to the $B = 0$ case is restored. Two representative I-V_{sd} cuts of Figs. 4(a) and 4(b) at $V_g = -7.3$ V are detailed in the corresponding insets, along with the I-V_{sd} curves at $V_g = 0$. The observed highly nonlinear transport behavior is yet another evidence of the Anderson localization of the helical states driven by the B field and contrasts with the almost linear current-voltage response in the TRS $B = 0$ case (see Supplemental Material [47], Figs. 4, 9–11).

In conclusion, through the low-temperature magneto-resistance measurements we were able to directly demonstrate the actual strength of topological protection in one-dimensional helical edge states of HgTe-based topological insulators. Breaking the TRS with an external magnetic field allowed us to expose the hallmark Anderson localization features for the edge states the exponential T dependence, giant reproducible mesoscopic fluctuations, and the gap-opening-like features in the I-V_{sd} characteristics. Our observation of identical behavior of the edges independently of their resistance in the finite B, strongly suggests the loss of topological protection at broken TRS. At the same time, the tremendous $G(T)$ dependence of the edges in $B \neq 0$, almost absent in zero B, highlights the distinct action of TRS breaking compared to other mechanisms, which enable backscattering in $B = 0$. The observation of ballistic transport via helical edge states strongly depends on the material, its quality, may be even sample dependent and presently does not go beyond edges several micrometers long. Our experiment demonstrates that for resistive edges the topological protection is still there in the time-reversal symmetric case perfectly sustaining the edge transport from localization.

---

*tikhonov@issp.ac.ru

[1] F. Bloch, Z. Phys. **52**, 555 (1929).

[2] Y. Kuga and A. Ishimaru, J. Opt. Soc. Am. A **1**, 831 (1984).

[3] M. P. Van Albada and A. Lagendijk, Phys. Rev. Lett. **55**, 2692 (1985).

[4] P.-E. Wolf and G. Maret, Phys. Rev. Lett. **55**, 2696 (1985).

[5] Y. V. Nazarov and Y. M. Blanter, *Quantum Transport: Introduction to Nanoscience* (Cambridge University Press, Cambridge, England, 2009).

[6] D. S. Wiersma, P. Bartolini, A. Lagendijk, and R. Righini, Nature (London) **390**, 671 (1997).

[7] T. Schwartz, G. Bartal, S. Fishman, and M. Segev, Nature (London) **446**, 52 (2007).

[8] P. A. Lee and T. V. Ramakrishnan, Rev. Mod. Phys. **57**, 287 (1985).

[9] H. Hu, A. Strybulevych, J. H. Page, S. E. Skipetrov, and B. A. van Tiggelen, Nat. Phys. **4**, 945 (2008).

[10] G. Roati, C. D'Errico, L. Fallani, M. Fattori, C. Fort, M. Zaccanti, G. Modugno, M. Modugno, and M. Inguscio, Nature (London) **453**, 895 (2008).

[11] J. Billy, V. Josse, Z. Zuo, A. Bernard, B. Hambrecht, P. Lugan, D. Clément, L. Sanchez-Palencia, P. Bouyer, and A. Aspect, Nature (London) **453**, 891 (2008).

[12] P. W. Anderson, Phys. Rev. **109**, 1492 (1958).

[13] E. Abrahams, P. W. Anderson, D. C. Licciardello, and T. V. Ramakrishnan, Phys. Rev. Lett. **42**, 673 (1979).

[14] M. Z. Hasan and C. L. Kane, Rev. Mod. Phys. **82**, 3045 (2010).

[15] X.-L. Qi and S.-C. Zhang, Rev. Mod. Phys. **83**, 1057 (2011).

[16] B. A. Bernevig, T. L. Hughes, and S.-C. Zhang, Science **314**, 1757 (2006).

[17] M. Konig, S. Wiedmann, C. Brune, A. Roth, H. Buhmann, L. W. Molenkamp, X.-L. Qi, and S.-C. Zhang, Science **318**, 766 (2007).

[18] I. Knez, R.-R. Du, and G. Sullivan, Phys. Rev. Lett. **107**, 136603 (2011).

[19] E. B. Olshanetsky, Z. D. Kvon, G. M. Gusev, A. D. Levin, O. E. Raichev, N. N. Mikhailov, and S. A. Dvoretsky, Phys. Rev. Lett. **114**, 126802 (2015).

[20] A. Roth, C. Brune, H. Buhmann, L. W. Molenkamp, J. Maciejko, X.-L. Qi, and S.-C. Zhang, Science **325**, 294 (2009).

[21] K. Suzuki, Y. Harada, K. Onomitsu, and K. Muraki, Phys. Rev. B **87**, 235311 (2013).

[22] T. Li, P. Wang, G. Sullivan, X. Lin, and R.-R. Du, Phys. Rev. B **96**, 241406(R) (2017).

[23] Z. Fei, T. Palomaki, S. Wu, W. Zhao, X. Cai, B. Sun, P. Nguyen, J. Finney, X. Xu, and D. H. Cobden, Nat. Phys. **13**, 677 (2017).

[24] S. U. Piatrusha, V. S. Khrapai, Z. D. Kvon, N. N. Mikhailov, S. A. Dvoretsky, and E. S. Tikhonov, Phys. Rev. B **96**, 245417 (2017).

[25] G. M. Gusev, E. B. Olshanetsky, Z. D. Kvon, N. N. Mikhailov, and S. A. Dvoretsky, Phys. Rev. B **87**, 081311(R) (2013).

[26] C. Brüne, A. Roth, H. Buhmann, E. M. Hankiewicz, L. W. Molenkamp, J. Maciejko, X.-L. Qi, and S.-C. Zhang, Nat. Phys. **8**, 485 (2012).

[27] G. M. Min'kov, A. A. Sherstobitov, A. V. Germanenko, O. E. Rut, S. A. Dvoretskii, and N. N. Mikhailov, JETP Lett. **101**, 469 (2015).

[28] G. M. Gusev, Z. D. Kvon, O. A. Shegai, N. N. Mikhailov, S. A. Dvoretsky, and J. C. Portal, Phys. Rev. B **84**, 121302(R) (2011).

[29] K. C. Nowack, E. M. Spanton, M. Baenninger, M. König, J. R. Kirtley, B. Kalisky, C. Ames, P. Leubner, C. Brüne, H. Buhmann, L. W. Molenkamp, D. Goldhaber-Gordon, and K. A. Moler, Nat. Mater. **12,** 787 (2013).

[30] L. Du, I. Knez, G. Sullivan, and R.-R. Du, Phys. Rev. Lett. **114,** 096802 (2015).

[31] S. Wu, V. Fatemi, Q. D. Gibson, K. Watanabe, T. Taniguchi, R. J. Cava, and P. Jarillo-Herrero, Science **359,** 76 (2018).

[32] K. Bendias, S. Shamim, O. Herrmann, A. Budewitz, P. Shekhar, P. Leubner, J. Kleinlein, E. Bocquillon, H. Buhmann, and L. W. Molenkamp, Nano Lett. **18,** 4831 (2018).

[33] R. de Picciotto, H. L. Stormer, L. N. Pfeiffer, K. W. Baldwin, and K. W. West, Nature (London) **411,** 51 (2001).

[34] G. M. Gusev, Z. D. Kvon, E. B. Olshanetsky, A. D. Levin, Y. Krupko, J. C. Portal, N. N. Mikhailov, and S. A. Dvoretsky, Phys. Rev. B **89,** 125305 (2014).

[35] E. S. Tikhonov, D. V. Shovkun, V. S. Khrapai, Z. D. Kvon, N. N. Mikhailov, and S. A. Dvoretsky, JETP Lett. **101,** 708 (2015).

[36] P. P. Aseev and K. E. Nagaev, Phys. Rev. B **94,** 045425 (2016).

[37] S. U. Piatrusha, L. V. Ginzburg, E. S. Tikhonov, D. V. Shovkun, G. Koblmüller, A. V. Bubis, A. K. Grebenko, A. G. Nasibulin, and V. S. Khrapai, JETP Lett. **108,** 71 (2018).

[38] X. Qian, J. Liu, L. Fu, and J. Li, Science **346,** 1344 (2014).

[39] L. Fu and C. L. Kane, Phys. Rev. Lett. **100,** 096407 (2008).

[40] C. Xu and J. E. Moore, Phys. Rev. B **73,** 045322 (2006).

[41] J. Maciejko, C. Liu, Y. Oreg, X.-L. Qi, C. Wu, and S.-C. Zhang, Phys. Rev. Lett. **102,** 256803 (2009).

[42] J. I. Väyrynen, M. Goldstein, and L. I. Glazman, Phys. Rev. Lett. **110,** 216402 (2013).

[43] N. Kainaris, I. V. Gornyi, S. T. Carr, and A. D. Mirlin, Phys. Rev. B **90,** 075118 (2014).

[44] J. Wang, Y. Meir, and Y. Gefen, Phys. Rev. Lett. **118,** 046801 (2017).

[45] J. I. Väyrynen, D. I. Pikulin, and J. Alicea, Phys. Rev. Lett. **121,** 106601 (2018).

[46] P. Novelli, F. Taddei, A. K. Geim, and M. Polini, Phys. Rev. Lett. **122,** 016601 (2019).

[47] See Supplemental Material at http://link.aps.org/supplemental/10.1103/PhysRevLett.123.056801 for additional device fabrication and measurement technique details, as well as for supporting experimental data.

[48] M. V. Durnev and S. A. Tarasenko, Phys. Rev. B **93,** 075434 (2016).

[49] M. Büttiker, Phys. Rev. B **38,** 9375 (1988).

[50] P. Delplace, J. Li, and M. Büttiker, Phys. Rev. Lett. **109,** 246803 (2012).

[51] O. Raichev, Ukr. J. Phys. **60,** 538 (2015).

[52] M. König, M. Baenninger, A. G. F. Garcia, N. Harjee, B. L. Pruitt, C. Ames, P. Leubner, C. Brüne, H. Buhmann, L. W. Molenkamp, and D. Goldhaber-Gordon, Phys. Rev. X **3,** 021003 (2013).

[53] E. Y. Ma, M. R. Calvo, J. Wang, B. Lian, M. Muhlbauer, C. Brune, Y. T. Cui, K. Lai, W. Kundhikanjana, Y. Yang, M. Baenninger, M. Konig, C. Ames, H. Buhmann, P. Leubner, L. W. Molenkamp, S. C. Zhang, D. Goldhaber-Gordon, M. A. Kelly, and Z. X. Shen, Nat. Commun. **6,** 7252 (2015).

[54] C. W. J. Beenakker, Rev. Mod. Phys. **69,** 731 (1997).

[55] V. T. Dolgopolov, G. V. Kravchenko, A. A. Shashkin, and S. V. Kravchenko, Phys. Rev. B **46,** 13303 (1992).

[56] Y. B. Khavin, M. E. Gershenson, and A. L. Bogdanov, Phys. Rev. B **58,** 8009 (1998).